Environmental Earth Sciences (2019) 78:33
https://doi.org/10.1007/s12665-018-8004-3

ORIGINAL ARTICLE

Geochemistry and genesis of geothermal well water from a carbonate–evaporite aquifer in Chongqing, SW China

Pingheng Yang[1,2,3] · Luo Dan[1] · Chris Groves[3] · Shiyou Xie[1]

Received: 16 May 2018 / Accepted: 17 December 2018

Abstract
Thermal water is an important natural resource. The hydrogeochemistry and geothermometry of thermal water from the Qianyi well (TWQW), which is associated with the Tongjing Warm Springs located in the Eastern Sichuan Fold Belts in Chongqing, SW China, was investigated. The reservoir of this region consists of upper and middle Triassic carbonate and evaporite rocks. The TWQW was of Ca–Mg–SO_4 type with water temperature of 47.3 °C. Plotting on the Giggenbach Na–K–Mg diagram indicates that the TWQW was immature due to a mixing of shallow karst groundwater and thermal water. The mixing model indicates that the TWQW was composed of 49% deep thermal water and 51% shallow karst groundwater. Geothermometers suggest a reservoir temperature of about 79 °C, locating this aquifer at a depth of ~ 2.5 km. The δD and $\delta^{18}O$ values plot near the local meteoric water line, suggesting that the TWQW originates from local meteoric water at recharge elevations of ~ 780–1160 m a.s.l.. A conceptual model of the genesis for Tongjing Warm Springs was developed. Rainfall infiltrates via karst outcrops in the elevated areas of the northern Tongluoxia anticline, extracts heat from reservoir rocks at depth, dissolves minerals and becomes thermal water. The thermal water is driven by gravity, flows through the carbonate–evaporite aquifer, and follows the Tongluoxia anticline of the Eastern Sichuan Fold Belts to the southwest. The thermal water ascends to the surface along the incision created by the Wentang River and mixes with shallow karst groundwater to create warm springs. This study may be relevant to other karst geothermal reservoirs in China.

Keywords Carbonate–evaporite · Thermal water · Reservoir temperature · Mixture fraction · Geothermometer · Tongjing, China

Introduction

Geothermal resources are extensively distributed in China with diverse categories and rich capacity (Wang et al. 2013). Since 2006, the Chinese government has encouraged the development of geothermal energy along with other renewable energy sources (Zheng et al. 2010). China was one of the five countries with the greatest installed capacity and the greatest annual energy use in 2010 (Lund et al. 2011). Hydrothermal systems are widely distributed in China (Kong et al. 2014; Lu et al. 2018). Among these hydrothermal resources, karst thermal reservoirs are thought to have great energy potential and more economical production value, thus the karst geothermics in China has attracted significant attention of researchers and developers (Pang et al. 2018). Kong et al. (2014) pointed out that deep karst aquifers containing hot water are the most ideal targets for development due to their favorable characteristics including high single-well yield, low salinity, easy reinjection, and fewer environmental impacts when exploited.

Southwest China's Chongqing municipality, with a population of 33.9 million, is known throughout the country for its thermal waters. The geothermal field of Chongqing is a non-volcanic karst hydrothermal system, which

✉ Pingheng Yang
pinghengyang@126.com

[1] Field Scientific Observation and Research Base of Karst Eco-environments at Nanchuan in Chongqing, Ministry of Natural Resources of the People's Republic of China, Chongqing Key Laboratory of Karst Environment, School of Geographical Sciences, Southwest University, Chongqing 400715, China

[2] Key Laboratory of Shale Gas and Geoengineering, Institute of Geology and Geophysics, Chinese Academy of Sciences, Beijing 100029, China

[3] Crawford Hydrology Laboratory, Department of Geography and Geology, Western Kentucky University, 1906 College Heights Blvd., Bowling Green, KY 42101, USA

Published online: 02 January 2019

is located in the eastern Sichuan Basin. The geothermal resources of the Sichuan Basin account for the highest portion (up to 31.2%) of the total geothermal resources in China (Wang et al. 2013). Li and Liu (2011) documented the presence of 107 proven thermal waters, including 26 spring groups, 16 mining waters, and 65 well waters within the city. The Nan Warm Springs, Bei Warm Springs and Dong Warm Springs in Chongqing have been explored for hundreds of years. However, historical thermal water resources in this region are becoming depleted due to excessive extraction and destruction of surrounding areas. Examples include the cessation of flow from the Xi Warm Springs in 1986, the drying up of the Nan Warm Springs and Xiao Warm Springs in the early 1990s, diminished flow and temperatures or the cessation of flow from the Dong Warm Springs, and considerable decreases in discharge, temperatures and water levels in the Bei Warm Springs (Li and Liu 2011).

Currently, with rapid growth of the economy, the people of Chongqing are demanding more thermal water resources, which will consequently intensify the exploitation. In this context, investigation and knowledge of thermal water resources in the city, particularly their hydrogeochemistry and genesis, will become increasingly important. Despite this interest, little literature has been published on the thermal waters in Chongqing, except for the work of Li and Liu (2011), Luo et al. (2006a, b), Cheng et al. (2015), Yang et al. (2017), and Xiao et al. (2018). They discussed the distribution, recharge, groundwater flow, discharge and geochemistry of thermal waters in Chongqing and offered insight into the thermal water resources available in this region.

The Tongjing Warm Springs include warm springs and drilling well waters which are famous scenic spots in Chongqing due to their clean water, high temperatures and excellent water quality for physical therapy and spa use. The thermal water from the Qianyi well (TWQW), one of the Tongjing thermal water resources, is now the main supply for commercial utilization (i.e., outdoor and indoor pools for swimming, physiotherapy and other health-care facilities). It attracts more than 400,000 bathers each year. In better understand the functioning of the thermal reservoir, the goal of this paper was to characterize the hydrogeochemistry of the TWQW, quantify the mixing fraction of cold water with the thermal water, determine the reservoir temperature, and describe the genesis of origin and migration for the thermal water. The present study contributes to a better understanding of the thermal waters in the region and will aid in the long-term planning, management and use of the thermal water resources of the Tongjing Warm Springs, and the karst thermal water in Chongqing. Moreover, the widespread middle-to-low temperature karst geothermal reservoirs in China (Kong et al. 2014), coupled with the prevalence of geothermal utilization worldwide, suggest that this study can help understand the genesis and better management of other karst reservoirs globally, in particular for China.

Description of the study area

Geographical setting

The Tongjing Warm Springs are located in the Wentang River canyon in Tongjing Town, approximately 40 km from the downtown area of Chongqing (Fig. 1a). In 1982, the area of the Tongjing Warm Springs was designated a scenic exploration and preservation region by the Chongqing Municipal Government.

The area has a subtropical humid monsoon climate with a mean annual air temperature and precipitation of 17.3 °C and 1152 mm, respectively. The majority of the annual precipitation (53%) falls in May through September. The Wentang River, functioning as the local base level of erosion, runs through the study area from west to east (Fig. 1b).

Regional geological and hydrogeological framework

The study area is in the Eastern Sichuan Fold Belts characterized by folds with an alternating anticline and syncline distribution trending NE–SW. In this region, there are anticlines including Libixia, Wengtangxia, Guanyinxia, Tongluoxia, and Mingyuexia from west to east (Fig. 1a). The topography often coincides with the folds: anticlines form ridges, while synclines form valleys (Yang et al. 2017).

The Tongjing Warm Springs are situated on the east limb of the southern Tongluoxia anticline (Fig. 1b). The geological succession outcropping from the anticline axis to the limbs is made up of (1) the lower Triassic Jialingjiang formation (T_1j) and middle Triassic Leikoupo formation (T_2l) composed of carbonate and evaporite rocks (gypsum and/or anhydrite), > 650 m thick; (2) the upper Triassic Xujiahe formation (T_3xj) characterized by sandstone and shale ranging 172–1090 m thick; (3) Jurassic shale and clayed mudstone with a thickness ranging 1402.7–2498 m (Zeng 2012). Only in the axis of the anticline is a large part of the carbonate eroded, which is completely confined by standstones and shales of the T_3xj (Fig. 1b, c; modified from Zeng 2012). Because of the well-developed karst, two subterranean rivers, three shallow karst springs, and a cluster of artesian warm springs (Tongjing Warm Spring) are dispersed through the region with a total discharge of 8641 m^3/day (Zeng 2012).

The geothermal water system in this area consists of a low-heat conductive cap (cover), a karstified reservoir, and an underlying semi-confining bed. The Jurassic shale and clayed mudstone and the sandstone and shale of T_3xj make

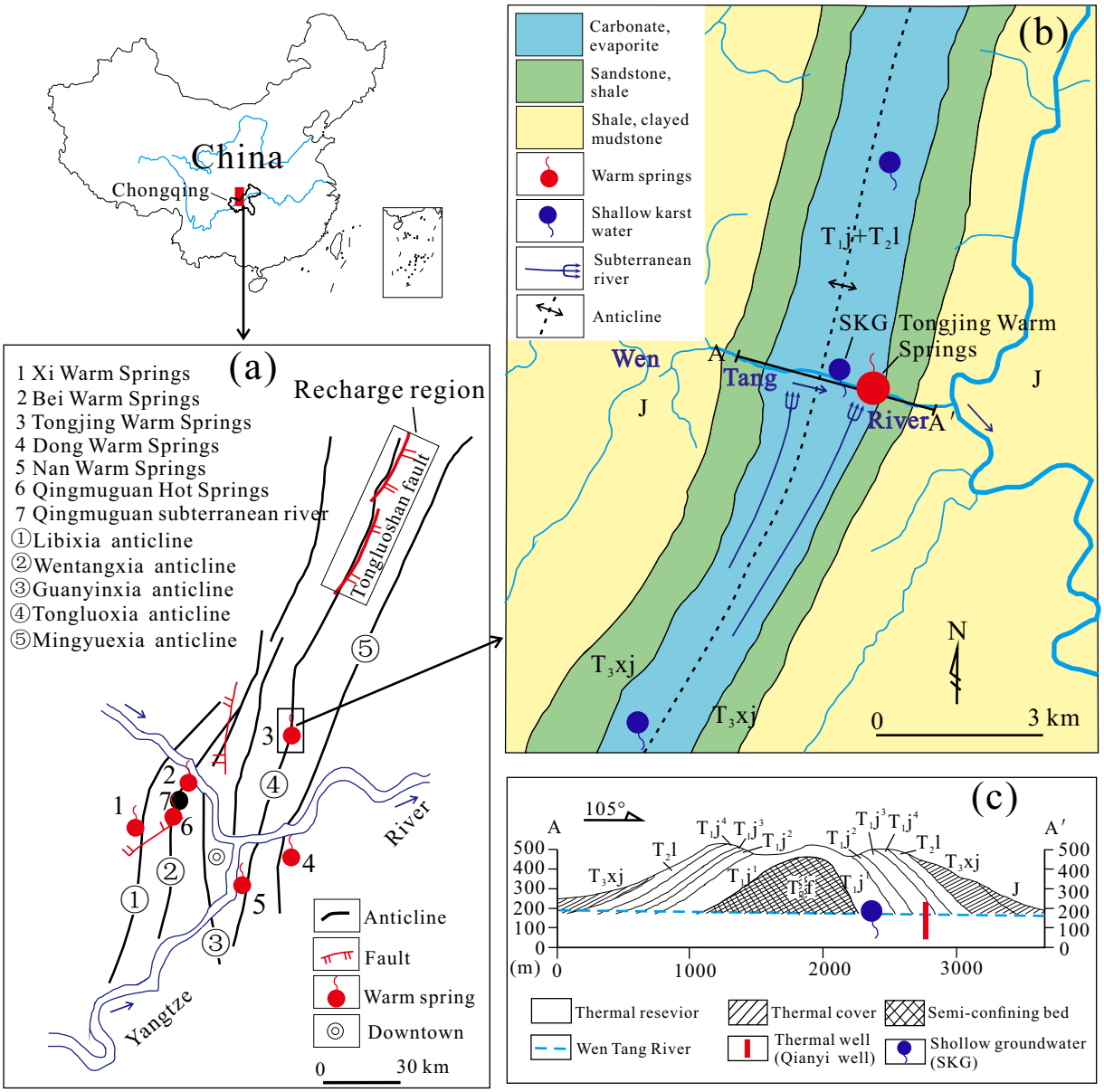

Fig. 1 **a** Map showing the geologic structure and thermal waters of the Eastern Sichuan Fold Belts. The Eastern Sichuan Fold Belts consist of a series of parallel anticlines and synclines trending NE–SW. **b** Hydrogeological sketch map of the area around the Tongjing Warm Springs. **c** Geologic section A–A′ crossing Tongjing Warm Springs. T_1f is the lower Triassic Feixianguan formation, mudstone interbedded with limestone, serving as the semi-confining bed underlying the thermal reservoir, $T_1j + T_2l$ is the lower Triassic Jialingjiang formation and middle Triassic Leikoupo formation, carbonate and evaporite rocks that form the thermal reservoir, T_3xj is the upper Triassic Xujiahe formation, sandstone and shale, forming the heat cover layer, J is the Jurassic formation, shale and clayed mudstone, also serving as a heat cover layer

up the overlying low-heat conductive cap characterized by low thermal conductivity. The T_2l and T_1j host the thermal reservoir characterized by karstification, high connectivity, and intense groundwater circulation. The lower Triassic Feixianguan formation (T_1f), unexposed in the surface (Fig. 1c) and consisting of mudstone interbedded with limestone, serves as the semi-confining bed underlying the thermal reservoir and is greater than 500 m thick. The regional terrestrial heat flow is ~ 50 mW/m^2, with an average thermal gradient of ~ 25°C/km with depth (Wang et al. 1990).

Qianyi well description

The thermal fluids of the Tongjing Warn Springs, which originally flowed out through artesian springs, now mainly flow from the Qianyi well. The total depth of the Qianyi well

is as much as 486 m with a surface elevation of 194 m a.s.l.. It was drilled into the carbonate–evaporite aquifer of the T_1j unit, starting from the Section III of T_1j (T_1j^3), through Section II of T_1j (T_1j^2), and ending at the upper portion of T_1j (T_1j^1) (Fig. 2). As the drilling log shows, T_1j^3 is primarily composed of thick-bedded limestone with thinner beds of dolomitic limestone and is 105 m thick. T_1j^2 consists of dolomitic limestone, limestone, and gypsum and/or anhydrite breccia with a thickness of 360 m. The T_1j^1 portion of the well consists of limestone and interbedded, thinner layers of argillaceous limestone and is 11 m thick.

The diameters of the Qianyi well range from 349.3 to 152.4 mm from top to bottom as shown in Fig. 2. A hydraulic conductivity value of 1.9 m/day was calculated for the aquifer based on measurements from a pumping test. During drilling of the well, drilling fluid was lost at a rate of 26 m^3/s at a depth of 61.8 m, and all of the drilling fluid escaped when a depth of 83.54 m was reached, without return of any cuttings. Small caves at depths of 175.14–175.64 m and 343.57–343.77 m were encountered during the drilling (Fig. 2). A maximum pumping rate of 3600 m^3/day was recommended as a result of pumping test.

Methodology

The thermal water samples were collected and physical and chemical measurements were conducted from the outflow of the Qianyi well. The implicit assumption is that the measured temperatures represent the subsurface bottom well temperature (with negligible experimental errors or at least very small errors as compared to the geothermometer errors) where the geothermal fluids equilibrated for its chemical and isotopic components and did not change since then (Verma and Santoyo 1997). A shallow karst groundwater (SKG; Fig. 1)

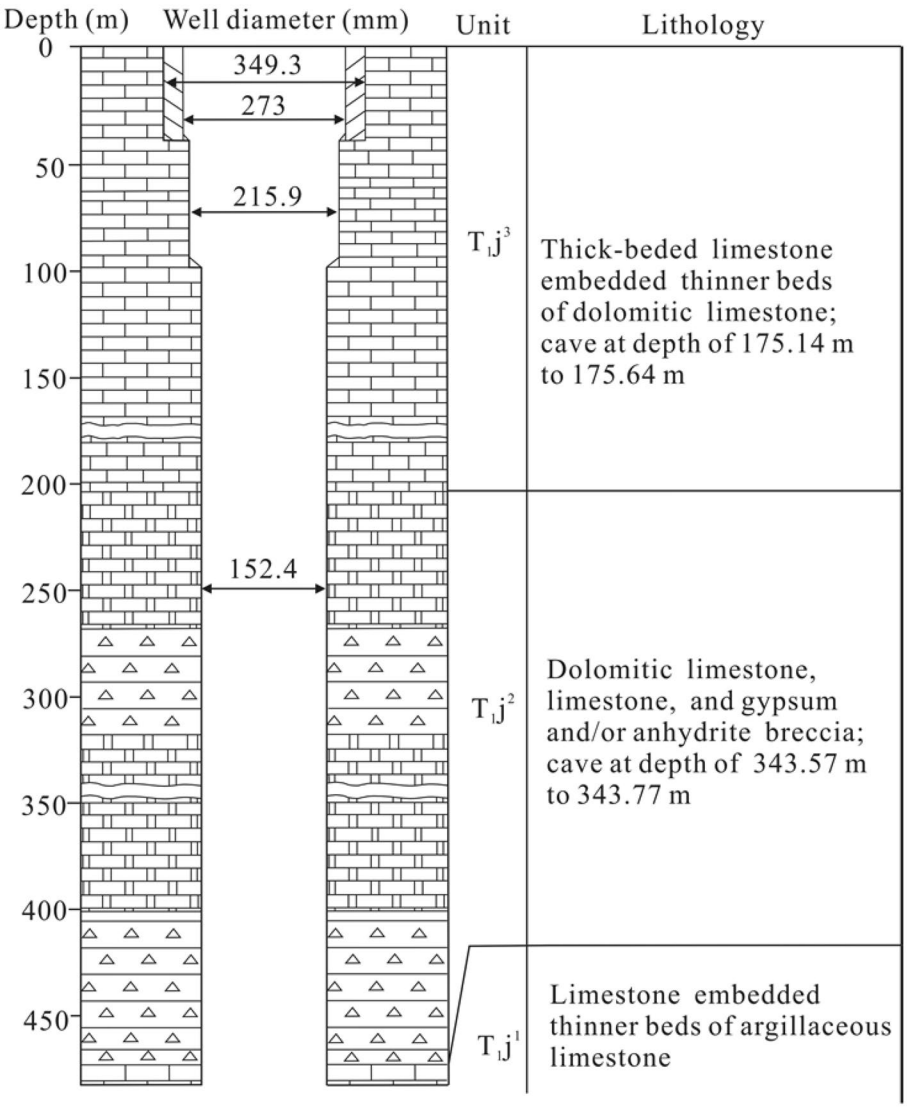

Fig. 2 Lithostratigraphic log for the Qianyi well

overlying the thermal reservoir was also sampled in comparison with the TWQW.

Field sampling

Water samples for cation analysis were collected in sterile 60-mL sample bottles. The samples were acidified to a pH of < 2 by adding two drops of ultrapure nitric acid in the field. The water samples for anion analysis were collected in 1-L polyethylene narrow-mouth, screw-cap bottles. Water samples for δD and $\delta^{18}O$ analyses were collected in 20-mL clean PETE bottles held underwater to prevent the inclusion of air bubbles. All water samples were refrigerated at 4 °C until analysis and were analyzed in the laboratory within 10 days of sampling.

Monthly water sampling was conducted from July 2014 through June 2015. Sampling of the SKG was conducted in July and August 2014 and April 2015 (Table 1).

Measurement of physical and chemical parameters

The pH, temperature and dissolved oxygen values of the TWQW and SKG were measured in situ using a WTW Multi-3430 (WTW Co., Ltd.) with the corresponding accuracies of 0.01 pH units, 0.1 °C and 0.01 mg/L, respectively. The HCO_3^- concentrations were titrated in the field using an alkalinity kit (Merck Co., Ltd.) with an accuracy of 0.1 mmol/L. The concentrations of cations were determined using an inductively coupled plasma optical emission spectrometer (PerkinElmer Ltd.) with a stability of RSD < 1% over 1 h and a standard deviation of RSD ≤ 0.5%. The concentrations of anions were measured using the GB/T 8538 – 1995 standard method (State Bureau of Technical Supervision of China 1995). The anion–cation balance was examined with relative errors of less than 5%. The concentration of total dissolved solid (TDS) was calculated from the cation and anion concentrations.

The δD and $\delta^{18}O$ were analyzed via an LGR laser spectroscopy, LWIA-30d liquid–water analyzer (Los Gatos Research, Inc.). Repeated analyses of several internal water standards showed that the precisions of δD and $\delta^{18}O$ measurements were better than 0.5‰ and 0.3‰, respectively. The results are reported in the delta (δ) notation relative to the V-SMOW standard and expressed in per mil (‰).

All measurements were conducted at the Laboratory of Geochemistry and Isotopes, Southwest University, Chongqing, China.

Results and discussion

Chemical composition

Table 1 lists the physical, chemical and isotopic composition of both the TWQW and SKG. Because thermal water mixed with the overlying SKG as it moved upward (described in detail in "Mixing fraction of shallow karst groundwater"), it is necessary to describe the physical and chemical properties of the SKG. The physical and chemical compositions of the TWQW were remarkably stable, as were those of the shallow karst groundwater (Table 1).

Chemical composition of the overlying karst groundwater

The SKG had an average water temperature of 17.4 °C and a pH of 7.3, indicating a weak alkaline pH. Among the cations, Ca^{2+} had the highest concentration, with an average of 104 mg/L (5.19 meq/L) and represented 74.8% of the total cations. Mg^{2+} had the second highest concentration, with an average of 19.8 mg/L (1.63 meq/L) and represented 23.5%. Small amounts of Na^+, K^+ and Sr^{2+} were also present in the water. Among the anions, HCO_3^- had the highest concentration, with an average of 323.3 mg/L (5.3 meq/L), and represented 78.6% of the total anions. SO_4^{2-} had the second highest concentration, with an average of 61 mg/L (1.27 meq/L), and represents 18.8%. Small amounts of Cl^- and NO_3^- were also present. Therefore, the hydrochemical facies of SKG was of Ca–Mg–HCO_3 (Fig. 3), which is one of the typical geochemical facies in karst environments (Ford and Williams 2007). The dissolved oxygen and SiO_2 concentrations of the water were 7.72 mg/L and 5.37 mg/L, respectively. A TDS of 530 mg/L indicates that the sample was fresh water. The mean values of $\delta^{18}O$ and δD were − 8.91‰ and − 59.79‰, respectively.

Chemical composition of the thermal water

The mean water temperature of the TWQW was 47.3 °C, and the pH was 6.8, indicating a neutral pH. Among the cations, the Ca^{2+} concentration was the highest, 513 mg/L (25.6 meq/L), which represented 66.6% of the total cations. The Mg^{2+} concentration was the second highest, 106.9 mg/L (8.8 meq/L) and represented 22.9%. The concentrations of Na^+ and K^+ were 62.9 mg/L (2.74 meq/L) and 37.7 mg/L (0.96 meq/L), respectively, and these cations represented 7.1% and 2.5% of the total cations, respectively. The Sr^{2+} concentration was 13.7 mg/L (0.31 meq/L). Among the anions, SO_4^{2-} had the highest concentration, 1521 mg/L (31.69 meq/L), and represented 88.2% of the total anions. HCO_3^-, unlike as a dominant anion in the SKG, had the second highest concentration, 209.4 mg/L (3.43 meq/L), and represents 9.4%. Small amounts of Cl^- and NO_3^- were also present. The dissolved oxygen and SiO_2 concentrations in the water were 2.55 mg/L and 16.81 mg/L, respectively. The thermal water was of Ca–Mg–SO_4 type (Fig. 3).

Carbonate thermal waters are frequently characterized by high Ca^{2+} and SO_4^{2-} concentrations due to dissolution of gypsum and/or anhydrite in the host rock (Goldscheider

Table 1 Physical, chemical and isotopic compositions of the TWQW and SKG in Chongqing, SW China

Sampling site	Sampling date	*T*	pH	SO_4^{2-}	HCO_3^-	Cl^-	NO_3^-	Ca^{2+}	Mg^{2+}	K^+	Na^+	Sr^{2+}	$\delta^{18}O$	δD	SiO_2	DO	TDS
TWQW	7/29/2014	47.2	6.77	1510	207	30	0.68	512	106.4	37.2	63.4	13.74	−7.69	−50.3	16.8	2.55	2481
	8/20/2014	47.2	6.85	1530	207	30.1	0.68	512	107.2	38.2	62.6	13.75	−8.53	−58.5	16.8	2.55	2502
	9/18/2014	47.2	6.79	1530	214	30.1	0.67	512	106.2	37.7	62.1	13.72	−8.22	−56.9	16.8	2.54	2500
	10/18/2014	47.3	6.84	1520	207	30.3	0.67	514	107.3	38.1	62.7	13.69	−8.19	−56.3	16.8	2.55	2494
	11/21/2014	47.3	6.81	1520	214	30.1	0.67	516	106.9	38.4	63.5	13.76	−8.00	−52.8	16.8	2.55	2497
	12/27/2014	47.2	6.77	1520	207	30.1	0.67	512	107.1	37.5	63.2	13.70	−7.94	−52.0	16.8	2.55	2492
	1/20/2015	47.2	6.78	1550	207	30.2	0.68	512	106.5	37.5	62.9	13.71	−7.85	−51.7	16.8	2.54	2520
	2/25/2015	47.4	6.76	1520	214	30.2	0.67	514	107.5	37.6	62.8	13.68	−8.16	−54.8	16.8	2.55	2488
	3/16/2015	47.3	6.72	1520	207	30.3	0.68	514	107.1	37.7	63.1	13.72	−8.56	−59.4	16.8	2.56	2494
	4/15/2015	47.3	6.75	1510	214	30.2	0.68	514	107.3	37.2	63.3	13.77	–	–	16.8	2.55	2484
	5/20/2015	47.3	6.78	1520	207	30.1	0.68	512	107.2	37.1	62.7	13.73	−9.01	−60.6	16.8	2.54	2492
	6/21/2015	47.2	6.82	1500	207	31.1	0.67	510	106.5	37.6	62.4	13.71	−9.12	−61.8	16.8	2.54	2470
Mean values	–	47.3	6.79	1521	209	30.2	0.67	513	106.9	37.7	62.9	13.70	−8.23	−55.5	16.8	2.55	2493
SKG	7/29/2014	17.3	7.3	60	323	3.6	4.62	104	19.7	3.1	4.1	0.68	−8.92	−59.82	5.36	7.76	523
	8/25/2014	17.5	7.31	61	323	3.5	4.60	104	19.8	3	4	0.67	−8.91	−59.77	5.37	7.80	524
	4/15/2015	17.5	7.29	61	323	3.6	4.61	104	19.9	3.1	4.2	0.67	−9.22	−62.36	5.38	7.61	543
Mean values	–	17.4	7.3	61	323	3.6	4.61	104	19.8	3.1	4.1	0.7	−8.91	−59.79	5.37	7.72	530

Concentrations of major irons, TDS and dissolved oxygen (DO) in mg/L, water temperature (*T*) in °C, $\delta^{18}O$ and δD in ‰

– No data

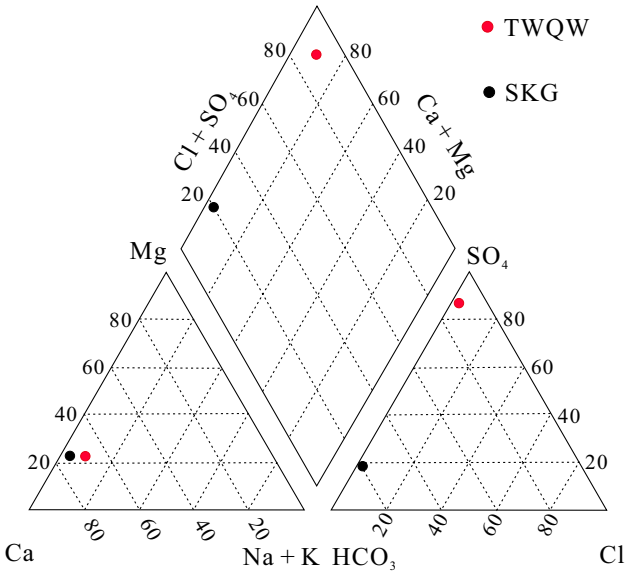

Fig. 3 Piper plot of the TWQW and SKG in Chongqing, SW China. Due to stabilization, all physical and chemical data overlap in the plot

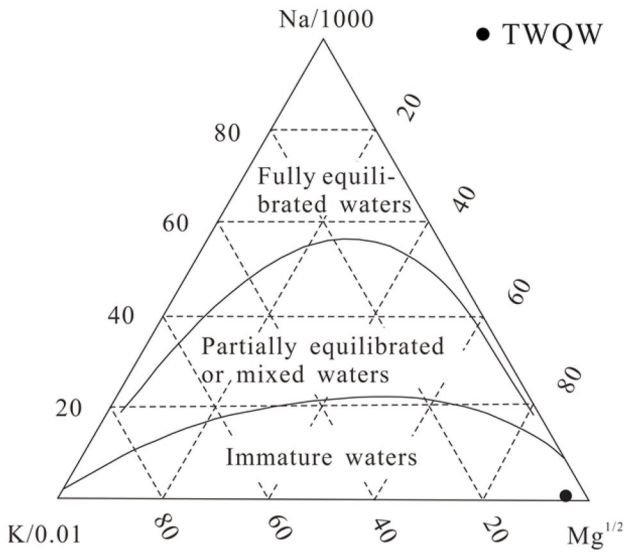

Fig. 4 The TWQW plotted on the Na–K–Mg diagram of Giggenbach (1988). The TWQW is immature due to the mixing of the deep thermal water and shallow karst groundwater. Due to stabilization, all physical and chemical data overlap in the plot

et al. 2010; Yang et al. 2017; Xiao et al. 2018). The gypsum and anhydrite minerals develop in the well at depth (Fig. 2). The high Ca^{2+} and SO_4^{2-} concentrations in the TWQW, therefore, are derived from the dissolution of gypsum and anhydrite in the host rock, which is confirmed by Xiao et al. (2018) using sulfate isotope in Qingmuguan Warm Springs and Bei Warm Springs (Fig. 1a). The relatively lower HCO_3^- concentrations in TWQW are ascribed to the common ion effect (Jin et al. 2010; Yang et al. 2017), which is characterized by a higher concentration of Ca^{2+} derived from the dissolution of gypsum and/or anhydrite strongly inhibiting the dissolution of carbonate (calcite and dolomite). Notably, the TDS in TWQW was 2493 mg/L, almost five times that of the SKG, indicating that the TWQW is brackish. The δD and $\delta^{18}O$ values of the TWQW ranged from 50.3 to 61.8‰ and from 7.7 to 9.1‰, respectively, with mean values of −55.5‰ and −8.2‰, respectively.

Mixing fraction of shallow karst groundwater

The Na–K–Mg diagram of Giggenbach (1988) has been widely used to evaluate the water–rock equilibrium in thermal waters. Based on its hydrochemistry, the TWQW was plotted on a Na–K–Mg diagram (Fig. 4). The water plotted in the immature field, suggesting the addition of a significant quantity of cold water (shallow karst groundwater) as the deep hot (thermal) water moves upward, which is typical of such systems worldwide (e.g., Pastorelli et al. 1999; Pirlo 2004; Cruz and Franca 2006; Tassi et al. 2010; Cinti et al. 2011; Guo and Wang 2012). This finding makes it important to calculate how much cold water is mixed with the deep hot water during its upwelling.

The thermal water ascends from depth along a permeable channel and, from a certain initial temperature, cools during this ascent. The rising deep hot water encounters cold water from a permeable stratum, and pressure induces the cold water to enter the deep hot water channel (e.g., Audra et al. 2010; Stober et al. 2016). Subsequently, the mixed water flows from the ground and discharges as warm springs, or well waters. The SiO_2 dissolved by the deep hot water in the deep reservoir follows the quartz solubility curve, and higher temperatures result in greater SiO_2 solubility (Fournier and Truesdell 1974). The oversaturated SiO_2, however, does not precipitate out of the thermal water with decreasing temperature (unlike when the amorphous SiO_2 solubility is reached). Thus, the thermal water can "remember" its initial high temperatures (Fournier and Truesdell 1974). Accordingly, the cold–hot water mixing inevitably causes the initial enthalpy and initial SiO_2 concentration of the deep hot water to drop to the final enthalpy and SiO_2 concentration of the thermal water. If the thermal water is saturated in dissolved SiO_2, the temperature and SiO_2 concentration in the thermal water are two different functions of the initial enthalpy of the thermal water, as expressed below (Fournier and Truesdell 1974):

$$S_c X + S_h(1 - X) = S_t, \quad (1)$$

$$SiO_{2c} X + SiO_{2h}(1 - X) = SiO_{2t}, \quad (2)$$

where S_c is the enthalpy of the cold water, S_h is the enthalpy of the deep hot water, S_t is the enthalpy of the thermal water,

SiO_{2c} is the SiO_2 concentration of the cold water, SiO_{2h} is the SiO_2 concentration of the deep hot water, SiO_{2t} is the SiO_2 concentration of the thermal water, and X is the mixture fraction of the cold water and deep hot water.

In Eqs. (1) and (2), only the cold water mixture fraction and the initial enthalpy of the deep hot water are unknown. The direct solution of these equations would be complex. However, the solutions can be calculated using a diagrammatic method. According to Eqs. (1) and (2), the solutions of the cold water mixing fraction X can be obtained as follows (Fournier and Truesdell 1974):

$$X1 = (S_h - S_t)/(S_h - S_c) \quad (3)$$

and

$$X2 = (SiO_{2h} - SiO_{2t})/(SiO_{2h} - SiO_{2c}). \quad (4)$$

Here, $X1$ and $X2$ are the two solutions of the mixture fraction of cold water to deep hot water. The other symbols are the same as those defined earlier. The point of intersection gives the estimated temperature of the reservoir and the fraction of cold water.

The SiO_2 concentration of TWQW (SiO_{2t}) used in the calculation is the measured concentration of 16.8 mg/L. This concentration demonstrates the thermal water is slightly saturated in dissolved SiO_2 relative to quartz, and is far undersaturated in amorphous SiO_2, which is suggested by the relationship between temperature and SiO_2 (Fig. 5). The SiO_2 concentration of the cold water (SiO_{2c}) was 5.37 mg/L, obtained from the SKG. The enthalpies of the cold water (S_c) and thermal water (S_t) are obtained from Table 2 based on the temperatures of 18.5 °C and 47.3 °C of SKG and TWQW, respectively. Each of the enthalpies and SiO_2 concentrations corresponding to the various temperatures in Table 2 were substituted in Eqs. (3) and (4) to produce the mixing proportion of cold water and to plot the diagram in Fig. 6. As shown in Fig. 6, the point of interpolated intersection of X1 and X2 shows that the 51% of shallow karst groundwater mixes with 49% of deep hot water. The fraction of the shallow karst groundwater is much lower than that of some karst geothermal systems (e.g., Lu et al. 2018). Karst sinkholes, shafts and fissures that connect the surface and shallow groundwater are common in the Eastern Sichuan Fold Belts (Yang et al. 2013, 2017). In addition, subterranean rivers are widely distributed in Chongqing, which are abundant in shallow karst groundwater (Pu et al. 2012). These karst features allow the rising deep hot water to mix with cold shallow karst groundwater.

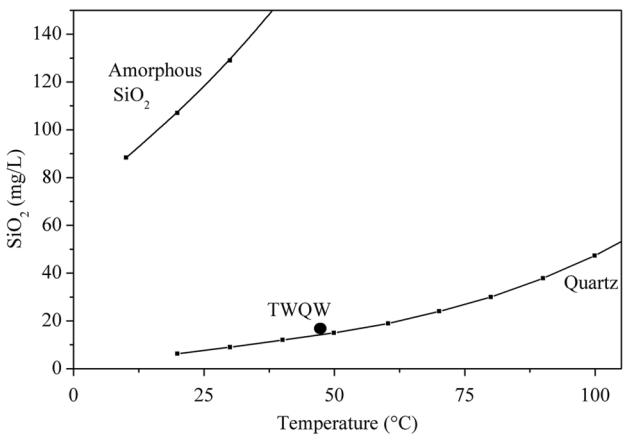

Fig. 5 Temperature vs. SiO_2 graph indicating the dissolved SiO_2 of the TWQW is slightly saturated and amorphous SiO_2 is far undersaturated (modified from Majumdar et al. 2009). Due to stabilization, all physical and chemical data overlap in the plot

Table 2 Enthalpies of water and quartz solubilities at selected temperatures (Fournier and Truesdell 1974)

Temperature (°C)	Enthalpy (×4.1868 J/g)	SiO_2 (mg/L)
50	50	13.5
75	75	26.6
100	100.1	48
125	125.4	80
150	151	125
175	177	185
200	203.6	265
225	230.9	365
250	259.2	486
275	289	614
300	321	692

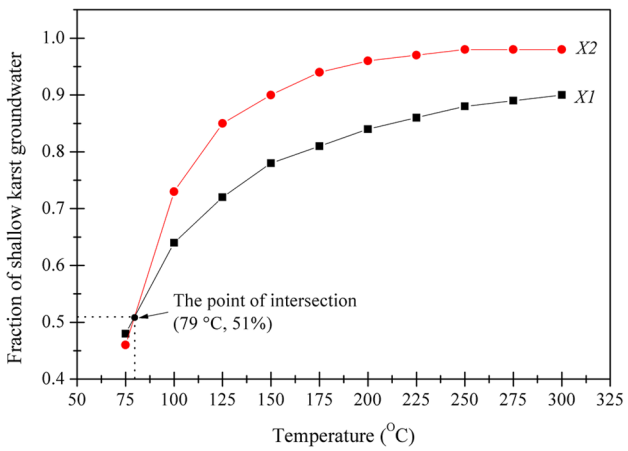

Fig. 6 A mixing model indicates the fraction of shallow karst groundwater and calculated reservoir temperature. The point of interpolated intersection of X1 (black line with squares) and X2 (red line with circles) gives the estimated temperature of the reservoir and the fraction of cold water. The value of the horizontal dotted line indicates 51% of the SKG mixing the hot water at depth, and the value of the vertical dotted line represents 79 °C of the reservoir temperature

Thermal reservoir temperature

The thermal reservoir temperature is a crucial parameter in evaluating the potential of a geothermal field to utilize as a possible source of energy. Due to the above-mentioned mixing of shallow karst groundwater and deep hot water, the measured temperature at the outflow of the well in situ does not represent the real original temperature of the heat reservoir, an important parameter indispensable for evaluating geothermal resources. From the mixing model, the reservoir temperature is approximately 79 °C (Fig. 6).

Moreover, it is possible to calculate the reservoir temperature using a geothermometer, which assumes that hydrothermal fluids will reach chemical equilibrium with minerals under the reservoir temperature and this equilibrium remains even when the temperature of the thermal water decreases during its upward movement (Pirlo 2004).

Geothermometers presently used include cation geothermometers, e.g., K–Mg (Giggenbach 1988), Na/K (Ibrahim 2002), Na–K–Ca (Fournier and Truesdell 1973) and Na–Li thermometers (Fouillac and Michard 1981), silica (quartz and chalcedony) geothermometers (Fournier 1977), isotope geothermometers (Millot and Négrel 2007) and gas geothermometers (D'Amore et al. 1993). Since TWQW was immature and a result of the mixing of deep hot water and shallow karst groundwater (Fig. 4), the cation geothermometer cannot be applied reliably to calculate the reservoir temperature. In this study, the silica-based geothermometer described by Fournier (1977) was selected to calculate the reservoir temperature.

Table 3 presents the calculated reservoir temperatures based on a silica geothermometer. The temperature from amorphous silica resulted in an unreliable negative value, which is attributed to the far unsaturation with respect to amorphous silica (Fig. 5). It is theoretically reliable to estimate the reservoir temperature using a quartz thermometer (Fournier 1977) in the carbonate reservoir of Chongqing (Yang et al. 2017). However, the temperatures resulting from quartz geothermometers were much lower relative to the reservoir temperature calculated by the mixing model mentioned above. This is mainly because the contribution of SiO_2 concentration in the mixing shallow karst groundwater to the deep hot water is not excluded. It is therefore necessary to eliminate the mixing fraction of shallow karst groundwater and restore the real SiO_2 concentration of the reservoir. According to the shallow karst groundwater mixing fraction of 51% during the upward movement of thermal water, the pre-mix initial SiO_2 concentration in the reservoir can be substituted into the respective silica geothermometers to calculate the initial reservoir temperature. The reservoir temperature can also be inverted by deducting the mixing fraction of shallow karst groundwater from the measured temperature in situ at the spring outlet, as given in Table 3. The restored temperatures from quartz-no steam loss (77.6 °C) and quartz-maximum after steam loss (81.5 °C) are nearly the same temperatures as the results from the methods of recovered measurement in situ (76.3 °C) and mixing model (79 °C). As such, the reservoir temperature used for the study area is assigned a mean value of 79 °C based on the four methods mentioned above. The calculated reservoir temperature of the study site is confirmed by a geological survey in Chongqing with a range of 64–104 °C (average 84 °C; Chongqing Municipal People's Government 2010) and the main urban areas of Chongqing with a range of 64.8–93.4 (average 82 Yang et al. 2017). In addition, the reservoir temperature of the study site is similar to that of other karst reservoir temperatures, such as in Tangshan, Nanjing (Lu et al. 2018), and northern Jinan, China (Wang et al. 2015).

Table 3 Reservoir temperatures based on different methods

Method	*T*	Restored *T*
Quartz-no steam loss (Fournier 1977)	57	77.6
Quartz-maximum after steam loss (Fournier 1977)	63.2	81.5
Amorphous silica (Fournier 1977)	−51.3	−34.4
Mixing model (Fournier and Truesdell 1974)	89	–
Measured temperature in situ	47.5	76.3

Temperature (*T*) in °C

Circulation depth of the thermal water

The groundwater circulation depth is an important constraint on the thermal water temperature. Assuming that the elevated temperature of the thermal water is due to heating during deep circulation, the circulation depth of the thermal water was calculated based on the reservoir temperature. The circulation depth of the thermal water was obtained using the following equation:

$$d = (t - t_0)/a + h, \tag{5}$$

where d is the reservoir circulation depth in km, t is the reservoir temperature in °C, t_0 is the local average annual air temperature in °C, a is the geothermal gradient in °C/km, and h is the depth of the constant temperature zone in km.

The reservoir temperature (t) is roughly taken as 79 °C. The local mean annual air temperature (t_0) is 17.3 °C, and the geothermal gradient (a) in Chongqing is thought to be 25 °C/km (Wang et al. 1990). The depth of the constant temperature zone is arbitrary to some extent and assumed to be 0.03 km. Thus, Eq. 5 yields a reservoir circulation depth of 2.5 km below the region. In 1983, well Tong-5 was drilled approximately 2.5 km east of the Qianyi well by the Sichuan Petroleum Administration to explore for natural gas in the

Carboniferous strata in the area. A hydraulic connection was shown to exist between Tongjing Hot Springs and Tong-5 (Luo 2000). Deep thermal water at a stable temperature of 62 °C was encountered at depth ranging 1763–2003 m. Artesian flow from well Tong-5 was as much as 7200 m^3/day (Luo 2000). Therefore, if the reservoir temperature at a depth of 1.76 km is 62 °C, a reservoir temperature of 79 °C is likely at a depth of 2.4 km. This estimation is consistent with the calculated reservoir circulation depth of 2.5 km described in the previous section and confirms that the estimated reservoir temperature of 79 °C is quite reasonable.

Elevation and temperature of the recharge zone based on isotopic composition

Condensation and evaporation cause different degrees of isotopic fractionation in natural waters during the transport of water masses, leading to characteristic δD and $\delta^{18}O$ values (Craig 1961; Timsic and Patterson 2014). Since the global meteoric water line (GMWL) was established by Craig in 1961 (Craig 1961), δD and $\delta^{18}O$ values have been widely used to study water circulation. The effects of altitude (Dansgaard 1964) and temperature (Yao et al. 1996) on δD and $\delta^{18}O$ values can be used to estimate the elevation and annual air temperature of the recharge area.

The δD and $\delta^{18}O$ values of the TWQW varied more than the physical and chemical parameters. The δD and $\delta^{18}O$ values of the TWQW plot along the Local Meteoric Water Line of Chongqing (Fig. 7, $\delta D = 8.3\ \delta^{18}O + 15.46$; Li et al. 2010), suggesting that the thermal water is recharged primarily by local meteoric water. This is consistent with other studies demonstrating meteoric origins for thermal water around the world (e.g., Lee et al. 2011; Moreira and Fernández 2015), especially in carbonate reservoirs (e.g., Goldscheider et al. 2010; Mao et al. 2015). Because no δD and $\delta^{18}O$ data are available for the local rain water, Eq. (6) (Zhou et al. 2010), which is commonly used in China, was used to calculate the elevation of the recharge area:

$$\delta D = -0.03\mathrm{ALT} - 27. \quad (6)$$

Here, ALT is the elevation of the recharge zone in m a.s.l..

The δD values were substituted in Eq. (6), yielding recharge elevations for the thermal water of 780–1160 m a.s.l. These recharge elevations agree well with the conclusions of Luo et al. (2006b), who estimated elevations of 800–1215 m for the recharge area of the Qingmuguan Warm Springs, which are located in a similar geological and hydrogeological setting in the Eastern Sichuan Fold Belts (Fig. 1a). The ^{14}C datum showed that the age of thermal water from well Tong-5 was 10,800 a (Luo 2000), which indicates that meteoric recharge occurred in the early Holocene (Kutzbach 1981; Hudspith et al. 2015). Due to some uncertainty in extrapolating the relationship between recharge altitude and isotopic concentration back through time, the calculated recharge elevations are therefore only considered broad estimations (Wang et al. 2015).

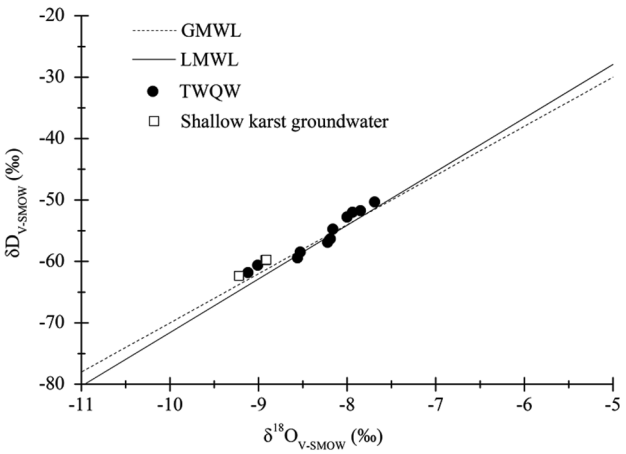

Fig. 7 δD and $\delta^{18}O$ diagram for TWQW and SKG in Chongqing, SW China. *GMWL* global meteoric water line ($\delta D = \delta^{18}O + 10$; Craig 1961); *LMWL* local meteoric water line of Chongqing ($\delta D = 8.3\ \delta^{18}O + 15.46$; Li et al. 2010)

The temperature effect of China's meteoric water δD values was calculated using the following equation (Zhou et al. 2010):

$$\delta D = 3T - 92, \quad (7)$$

where T is the mean annual air temperature of the recharge area in °C.

The resulting estimated mean annual air temperature of the recharge area is in the range of 10.1–13.9 °C. The mean NO_3^- concentration of 0.67 mg/L in the TWQW is significantly lower than that of the shallow karst groundwater (4.61 mg/L, Table 1). Nitrate is the most frequently introduced nutrient into groundwater systems from anthropogenic sources (Umezawa et al. 2008; Allums et al. 2012; Opazo et al. 2016). This difference in nitrate concentrations between TWQW and the SKG (Table 1) indicates that pristine ecologic environments are present in the recharge area.

The northern part of the Tongluoxia anticline, located north of the study site, shares similar geological structures and hydrogeological settings with the study area and exhibits the calculated elevations, mean annual air temperatures and ecologic environments. Because the δD and $\delta^{18}O$ values of TWQW plot near the local meteoric water line of Chongqing (Fig. 7), little or no evaporation has affected the thermal water. This further verifies that the recharge rainwater quickly percolates down to the groundwater zone. The setting that possesses such characteristics is most likely a karst area (Ford and Williams 2007). Therefore, we assume that the ~100 km northeastern end of the Tongluoxia anticline

(Fig. 1a), where karst outcrops are well developed, is the recharge zone for the thermal water in the study area.

Genesis model of Tongjing Warm Springs

Based on the geologic, hydrogeologic, and chemical framework of the study area (see above), the geothermal reservoir feeding the TWQW and nearby thermal water discharges is expected to be hosted in carbonate and evaporite rocks. Hence, we developed a conceptual model of the formation and migration of the thermal water in the Tongjing Warm Springs (Fig. 8). On a regional scale, groundwater movement from recharge to the discharge areas is generally gravity/topography driven (Tóth 1963; Jiang et al. 2012; Mádl-Szőnyi and Tóth 2015; Mádl-Szőnyi and Simon 2016), and thermal karst groundwater is associated with the regional groundwater flow systems (Ma et al. 2011). The presence of a structurally weak zone, such as a permeable fault, is more favorable for the percolation of meteoric water to depths (Chandrajith et al. 2013). There is a Tongluoshan fault extending from northeast to southwest with a length of approximated 60 km across the northeast Tongluoxia anticline (Fig. 1a). Carbonate rock outcrops are widely distributed in this area. The meteoric water percolates down into

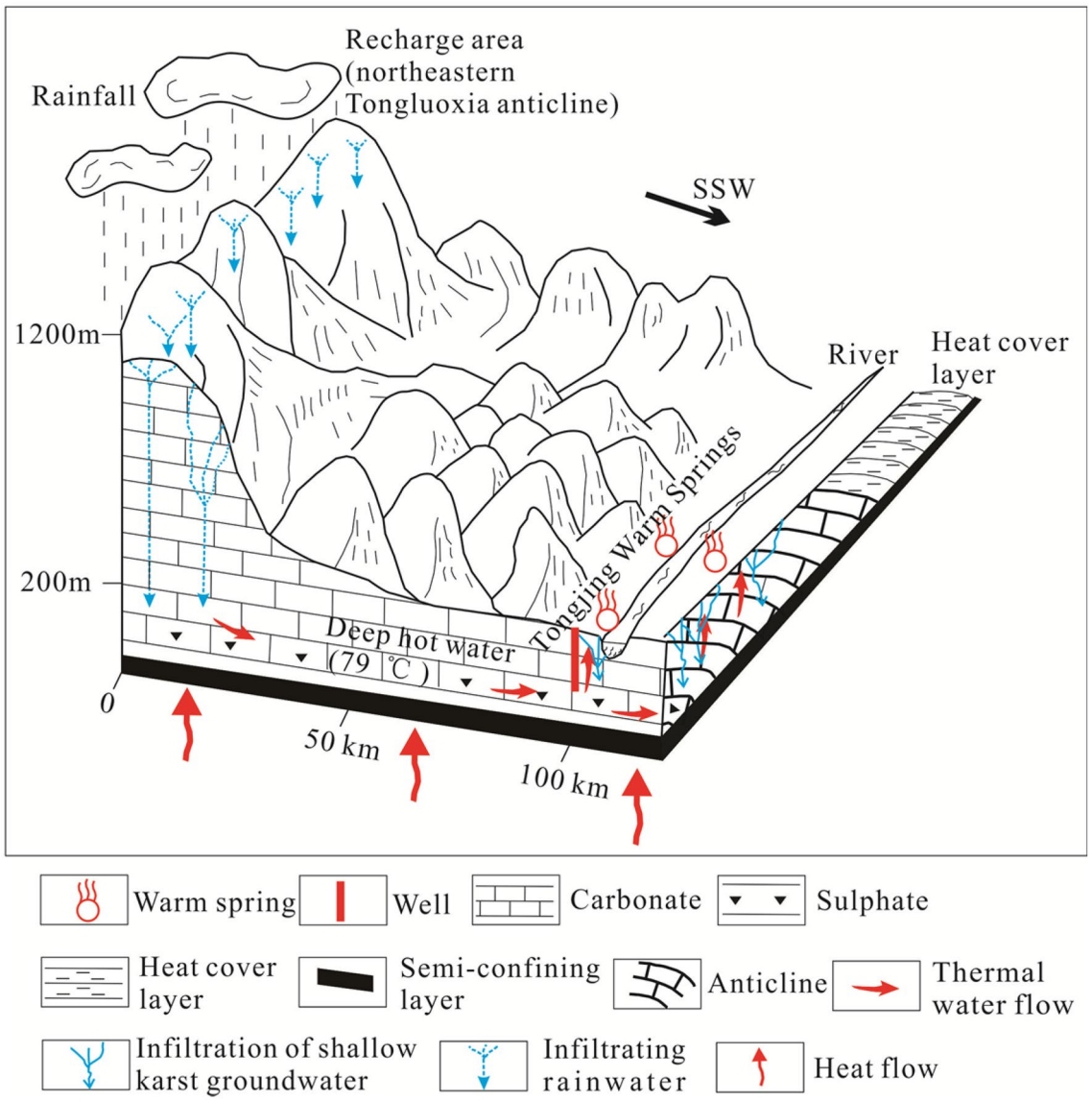

Fig. 8 Conceptual model of genesis for the hydrothermal system in the Tongjing Warm Springs which discharge from a regional groundwater flow system driven by gravity/topography. Rainwater infiltrates in the northeastern Tongluoxia anticline at elevations ranging 780–1160 m a.s.l. and descends to maximum depth of ~2.5 km below the region. The thermal water flows southward through the carbonate–evaporite aquifer and ascends to the surface along the incision created by the Wentang River or is drilled, and mixes with shallow karst groundwater to create warm springs. The carbonate and evaporite of T_1j+T_2l are exposed in the core of eroded anticlines

the karst aquifer through karst sinkholes, shafts, fissures and/or other permeable channels formed by the Tongluoshan fault connecting the surface to the subsurface at elevations of 780–1160 m a.s.l.. The water then percolates down into the carbonate and evaporite rocks of T_1j and T_2l, where it is heated by the rock. The carbonate–evaporite aquifer is limited at its base by the semi-confining and low-permeability mudstone interbedded with limestone of T_1f. It thus forms a deep circulation within the carbonate–evaporite rocks at a circulation depth of ~2.5 km below the region. The water temperature rises to 79 °C and becomes deep thermal water (Fig. 8). The substantial water–rock interaction between the deep thermal water and the surrounding rock causes a relatively high degree of mineralization, particularly including ions derived from the dissolution of gypsum and/or anhydrite, such as Ca^{2+} and SO_4^{2-}. Gypsum dissolution has produced significant porosity and permeability in the carbonate aquifer and this is an essential precursor to the development of karstic drainage (Gunn et al. 2006). Driven by the gravity/topography, the deep hot water originating from the recharge area is inferred to flow south-southward southwestward along the Tongluoxia anticline through the carbonate–evaporite aquifer of the T_2l and T_1j units.

Based on the observed structures and karst weathering, the shallow karst strata in the vicinity of the Tongjing Warm Springs contain abundant fissures, conduits, and channels connecting the surface and the aquifer. According to findings observed in the Qingmuguan karst subterranean river system, which shares a similar geological setting, karst fissures and other conduits can carry as much as 90% and 10% of the groundwater volume, respectively, in the shallow karst aquifer (Yang et al. 2013). The strata in the area of the Tongjing Warm Springs have been eroded by the Wentang River (Fig. 1c). This erosion has caused a reduction in aquifer pressure, thereby providing hydrodynamics favoring the presence of warm springs. The deep hot water ascends along the karst fractures and mixes with the shallow karst groundwater characterized by low-temperature, low-TDS, and relatively high bicarbonate and nitrate concentrations, lowering the water temperature from 79 to 47.5 °C (Fig. 8). Hence the TWQW and its nearby warm springs discharge from a regional groundwater flow system from the northeastern end of Tongluoxia anticline.

Conclusions

The geothermal reservoir feeding the TWQW and nearby thermal water discharges is expected to be hosted in carbonate–evaporite rocks. The hydrochemical facies of TWQW was of Ca–Mg–SO_4, whereas the overlying shallow karst groundwater was of Ca–Mg–HCO_3. The chemical composition of the TWQW was immature. Deep hot water mixes with shallow karst groundwater during its ascent from the reservoir. According to the mixing model, the warm water consists of 49% deep hot water and 51% cold shallow karst groundwater. The reservoir temperature was approximately 79 °C as calculated from the mixing model, recovered silica thermometers and in situ measurement with a reservoir circulation depth of ~2.5 km. The δD and $\delta^{18}O$ values of the TWQW suggest that the thermal water in the study area originates from local meteoric water at recharge elevations of 780–1160 m a.s.l. where mean annual air temperatures are 10.1–13.9 °C. This recharge likely occurs at the northeastern end of the Tongluoxia anticline, where karst outcrops are well developed. Due to force by gravity, the hot water flows southwestward along the Tongluoxia anticline and reaches the surface as warm springs or is drilled through wells in areas where a relatively low pressure of the aquifer was incised by the Wentang River.

The sampling campaigns were carried out during normal weather. However, the hydrogeochemistry of the shallow karst groundwater is greatly impacted by storm events, especially in areas influenced by subterranean rivers (e.g., Vesper and White 2004; Yang et al. 2013). The physics and chemistry of both TWQW and SKG may be representative of the chemistry along a longer time interval in normal weather. Nevertheless, the genesis of the thermal water in the study area is accurate with the exception of mixing fraction which influenced during extreme weather.

Acknowledgements We thank Brian Ham (Tennessee Department of Environment and Conservation, Division of Water Resources) for his constructive comments. This work was supported by the Fundamental Research Funds for the Central Universities (XDJK2018AB002), and the China Scholarship Council (CSC).

References

Allums SE, Opsahl SP, Golladay SW, Hicks DW, Conner LM (2012) Nitrate concentrations in springs flowing into the lower Flint River Basin, Georgia USA. J Am Water Resour Assoc 48:423–438. https://doi.org/10.1111/j.1752-1688.2011.00624.x

Audra P, D'Antoni-Nobecourt JC, Bigot JY (2010) Hypogenic caves in France. Speleogenesis and morphology of the cave systems. Bull Soc Geol Fr 181:327–335

Chandrajith R, Barth JAC, Subasinghe ND, Merten D, Dissanayake CB (2013) Geochemical and isotope characterization of geothermal spring waters in Sri Lanka: evidence for steeper than expected geothermal gradients. J Hydrol 476:360–369. https://doi.org/10.1016/j.jhydrol.2012.11.004

Cheng Q, Yang H, Zeng M (2015) The formation and protection of karst geothermal water resources in the main urban area of Chongqing. Carsologica Sinica 34:217–227. https://doi.org/10.11932/karst20150303 (in Chinese with English abstract)

Chongqing Municipal People's Government (2010) Geoglogical survey report of Chongqing, the capital of Warm Spring in China. Chongqing Municipal People's Government, Chongqing (in Chinese without English abstract)

Cinti D, Procesi M, Tassi F, Montegrossi G, Sciarra A, Vaselli O, Quattrocchi F (2011) Fluid geochemistry and geothermometry in the western sector of the Sabatini volcanic district and the Tolfa mountains (Central Italy). Chem Geol 284:160–181. https://doi.org/10.1016/j.chemgeo.2011.02.017

Craig H (1961) Isotopic variations in meteoric waters. Science 133:1702–1703

Cruz JV, França Z (2006) Hydrogeochemistry of thermal and mineral water springs of the Azores archipelago (Portugal). J Volcanol Geotherm Res 151:382–398. https://doi.org/10.1016/j.jvolgeores.2005.09.001

D'Amore F, Ramos-Candelaria MN, Seastres J Jr, Ruaya JR, Nuti S (1993) Applications of gas chemistry in evaluating physical processes in the Southern Negros (Palinpinon) geothermal field, Philippines. Geothermics 22:535–553. https://doi.org/10.1016/0375-6505(93)90035-L

Dansgaard W (1964) Stable isotopes in precipitation. Tellus 16:436–468. https://doi.org/10.1111/j.2153-3490.1964.tb00181.x

Ford DC, Williams PW (2007) Karst hydrogeology and geomorphology. Wiley Press, Chichester

Fouillac C, Michard G (1981) Sodium/lithium ratios in water applied to geothermometry of geothermal reservoirs. Geothermics 10:55–70. https://doi.org/10.1016/0375-6505(81)90025-0

Fournier RO (1977) Chemical geothermometers and mixing models for geothermal systems. Geothermics 5:41–50. https://doi.org/10.1016/0375-6505(77)90007-4

Fournier RO, Truesdell AH (1973) An empirical Na–K–Ca geothermometer for natural waters. Geochim Cosmochim Acta 37:1255–1275. https://doi.org/10.1016/0016-7037(73)90060-4

Fournier RO, Truesdell AH (1974) Geochemical indicators of subsurface temperature—2. Estimation of temperature and fraction of hot water mixed with cold water. J Res US Geol Surv 2:263–270. https://doi.org/10.3133/ofr741032

Giggenbach WF (1988) Geothermal solute equilibria. Derivation of Na–K–Mg–Ca geoindicators. Geochim Cosmochim Acta 52:2749–2765. https://doi.org/10.1016/0016-7037(88)90143-3

Goldscheider N, Mádl-Szőnyi J, Erőss A, Schill E (2010) Review: thermal water resources in carbonate rock aquifers. Hydrogeol J 18(6):1303–1318. https://doi.org/10.1007/s10040-010-0611-3

Gunn J, Bottrell SH, Lowe DJ, Worthington SRH (2006) Deep groundwater flow and geochemical processes in limestone aquifers: evidence from thermal waters in Derbyshire, England, UK. Hydrogeol J, 14: 868–881. https://doi.org/10.1007/s10040-006-0022-7

Guo Q, Wang Y (2012) Geochemistry of hot springs in the Tengchong hydrothermal areas, Southwestern China. J Volcanol Geotherm Res 215–216:61–73. https://doi.org/10.1016/j.jvolgeores.2011.12.003

Hudspith VA, Belcher CM, Kelly R, Hu FS (2015) Charcoal reflectance reveals early holocene boreal deciduous forests burned at high intensities. PLoS One 10:e0120835. https://doi.org/10.1371/journal.pone.0120835

Ibrahim C (2002) A new improved Na/K geothermometer by artificial neural networks. Geothermics 31:751–760. https://doi.org/10.1016/S0375-6505(02)00044-5

Jiang XW, Wan L, Ge S, Cao GL, Hou GC, Hu FS, Wang XS, Li HL, Liang SH (2012) A quantitative study on accumulation of age mass around stagnation points in nested flow systems. Water Resour Res 48:771–784. https://doi.org/10.1029/2012wr012509

Jin L, Siegel DI, Lautz LK, Mitchell MJ, Dahms DE, Mayer B (2010) Calcite precipitation driven by the common ion effect during groundwater-surface-water mixing: a potentially common process in streams with geologic settings containing gypsum. Geol Soc Am Bull 122:1027–1038. https://doi.org/10.1130/B30011.1

Kong Y, Pang Z, Shao H, Hu S, Kolditz O (2014) Recent studies on hydrothermal systems in China: a review. Geotherm Energy. https://doi.org/10.1186/s40517-014-0019-8

Kutzbach JE (1981) Monsoon climate of the early Holocene: climate experiment with the Earth's orbital parameters for 9000 years ago. Science 214:59–61. https://doi.org/10.1126/science.214.4516.59

Lee S, Kim T, Lee TJ (2011) Strontium isotope geochemistry and its geochemical implication from hot spring waters in South Korea. J Volcanol Geotherm Res 208:12–22. https://doi.org/10.1016/j.jvolgeores.2011.09.004

Li D, Liu D (2011) Geothermal reservoir structure and runoff flow recharge of geothermal water resources in Chongqing City. J Hohai Univ (Nat Sci) 39:372–376. https://doi.org/10.3876/j.issn.1000-1980.2011.04.004 (in Chinese with English abstract)

Li T, Li H, Shen C, Yang C, Li J, Yi C, Yuan D, Wang J, Xie S (2010) Study on the δD and $\delta^{18}O$ characteristics of meteoric precipitation during 2006–2008 in Chongqing. Adv Water Sci 21:757–764 (in Chinese with English abstract)

Lu L, Pang Z, Kong Y, Guo Q, Wang Y, Xu C, Gu W, Zhou L, Yu D (2018) Geochemical and isotopic evidence on the recharge and circulation of geothermal water in the Tangshan geothermal system near Nanjing, China: implications for sustainable development. Hydrogeol J 26:1705–1719. https://doi.org/10.1007/s10040-018-1721-6

Lund JW, Freeston DH, Boyd TL (2011) Direct utilization of geothermal energy 2010 worldwide review. Geothermics 40:159–180. https://doi.org/10.1016/j.geothermics.2011.07.004

Luo X (2000) Formation and characteristics of the geothermal spring in Tongjing scenic spot, North Chongqing district, Chongqing City. Carsologica Sinica 19:159–163 (in Chinese with English abstract)

Luo Y, Liu D, Liu X (2006a) System of the geothermal water in the Nanwenquan anticline. J Chongqing Univ (Nat Sci Ed) 29:131–158 (in Chinese with English abstract)

Luo Y, Liu D, Xu M (2006b) Study on the geothermal water runoff in Chongqing. Earth Environ 34:49–54 (in Chinese with English abstract)

Ma R, Wang YX, Sun ZY, Zheng CM, Ma T, Prommer H (2011) Geochemical evolution of groundwater in carbonate aquifers in Taiyuan, northern China. Appl Geochem 26:884–897. https://doi.org/10.1016/j.apgeochem.2011.02.008

Mádl-Szőnyi J, Simon S (2016) Involvement of preliminary regional fluid pressure evaluation into the reconnaissance geothermal-exploration—example of an overpressured and gravity-driven basin. Geothermics 60:156–174. https://doi.org/10.1016/j.geothermics.2015.11.001

Mádl-Szőnyi J, Tóth A (2015) Basin-scale conceptual groundwater flow model for an unconfined and confined thick carbonate region. Hydrogeol J 23:1359–1380. https://doi.org/10.1007/s10040-015-1274-x

Majumdar N, Mukherjee AL, Majumdar RK (2009) Mixing hydrology and chemical equilibria in Bakreswar geothermal area, eastern India. J Volcanol Geotherm Res 183:201–212. https://doi.org/10.1016/j.jvolgeores.2009.03.014

Mao X, Wang Y, Zhan H, Feng L (2015) Geochemical and isotopic characteristics of geothermal springs hosted by deep-seated faults in Dongguan Basin, Southern China. J Geochem Explor 158:112–121. https://doi.org/10.1016/j.gexplo.2015.07.008

Millot R, Négrel P (2007) Multi-isotopic tracing (δ^7Li, $\delta^{11}B$, $^{87}Sr/^{86}Sr$) and chemical geothermometry: evidence from hydro-geothermal systems in France. Chem Geol 244: 664–678. https://doi.org/10.1016/j.chemgeo.2007.07.015

Moreira P, Fernández RR (2015) La Josefina Au–Ag deposit (Patagonia, Argentina): a Jurassic epithermal deposit formed in a hot spring environment. Ore Geol Rev 67:297–313. https://doi.org/10.1016/j.oregeorev.2014.12.012

Opazo T, Aravena R, Parker B (2016) Nitrate distribution and potential attenuation mechanisms of a municipal water supply bedrock aquifer. Appl Geochem 73:157–168. https://doi.org/10.1016/j.apgeochem.2016.08.010

Pang Z, Kong Y, Shao H, Kolditz O (2018) Progress and perspectives of geothermal energy studies in China: from shallow to deep systems. Environ Earth Sci 77:580. https://doi.org/10.1007/s12665-018-7757-z

Pastorelli S, Marini L, Hunziker JC (1999) Water chemistry and isotope composition of the Acquarossa thermal system. Ticino Switz Geotherm 28:75–93. https://doi.org/10.1016/S0375-6505(98)00045-5

Pirlo MC (2004) Hydrogeochemistry and geothermometry of thermal groundwaters from the Birdsville Track Ridge, Great Artesian Basin, South Australia. Geothermics 33:743–774. https://doi.org/10.1016/j.geothermics.2004.07.001

Pu JB, Yuan DX, Zhang C, Zhao HP (2012) Identifying the sources of solutes in karst groundwater in Chongqing, China: a combined sulfate and strontium isotope approach. Acta Geol Sinica 86:980–992. https://doi.org/10.1111/j.1755-6724.2012.00722.x

State Bureau of Technical Supervision of China (1995) Method for examination of drinking natural mineral water (GB/T 8538 – 1995). State Bureau of Technical Supervision of China, Beijing (in Chinese without English abstract)

Stober I, Zhong J, Zhang L, Bucher K (2016) Deep hydrothermal fluid-rock interaction: the thermal springs of Da Qaidam, China. Geofluids 16:711–728. https://doi.org/10.1111/gfl.12190

Tassi F, Aguilera F, Darrah T, Vaselli O, Capaccioni B, Poreda RJ, Delgado Huertas A (2010) Fluid geochemistry of hydrothermal systems in the Arica-Parinacota, Tarapacá and Antofagasta regions (northern Chile). J Volcanol Geotherm Res 192:1–15. https://doi.org/10.1016/j.jvolgeores.2010.02.006

Timsic S, Patterson WP (2014) Spatial variability in stable isotope values of surface waters of eastern Canada and New England. J Hydrol 511:594–604. https://doi.org/10.1016/j.jhydrol.2014.02.017

Tóth J (1963) A theoretical analysis of groundwater flow in small drainage basins. J Geophys Res 68:4795–4812. https://doi.org/10.1029/Jz068i008p02354

Umezawa Y, Hosono T, Onodera S, Siringan F, Buapeng S, Delinom R, Yoshimizu C, Tayasu I, Nagata T, Taniguchi M (2008) Sources of nitrate and ammonium contamination in groundwater under developing Asian megacities. Sci Total Environ 404:361–376. https://doi.org/10.1016/j.scitotenv.2008.04.021

Verma SP, Santoyo E (1997) New improved equations for Na/K, Na/Li and SiO_2, geothermometers by outlier detection and rejection. J Volcanol Geotherm Res 79:9–23. https://doi.org/10.1016/S0377-0273(97)00024-3

Vesper DJ, White WB (2004) Storm pulse chemographs of saturation index and carbon dioxide pressure: implications for shifting recharge sources during storm events in the karst aquifer at Fort Campbell, Kentucky/Tennessee, USA. Hydrogeol J 12:135–143. https://doi.org/10.1007/s10040-003-0299-8

Wang J, Huang SY, Huang GS, Wang JY (1990) Basic characteristics of the Earth's temperature distribution in China. Seismological Press, Beijing

Wang G, Li K, Wen D, Lin W, Lin L, Liu Z, Zhang W, Ma F, Wang W (2013) Assessment of geothermal resources in China, In: Proceedings, thirty-eighth workshop on geothermal reservoir engineering, Stanford University, Stanford, California, February 11–13

Wang JL, Jin MG, Jia BJ, Kang FX (2015) Hydrochemical characteristics and geothermometry applications of thermal groundwater in northern Jinan, Shandong China Geothermics 57:185–195. https://doi.org/10.1016/j.geothermics.2015.07.002

Xiao Q, Jiang YJ, Shen LC, Yuan DX (2018) Origin of calcium sulfate-type water in the Triassic carbonate thermal water system in Chongqing, China: a chemical and isotopic reconnaissance. Appl Geochem 89:49–58. https://doi.org/10.1016/j.apgeochem.2017.11.011

Yang P, Yuan D, Ye X, Xie S, Chen X, Liu Z (2013) Sources and migration path of chemical compositions in a karst groundwater system during rainfall events. Chin Sci Bull 58: 2488–2496. https://doi.org/10.1007/s11434-013-5762-x

Yang P, Cheng Q, Xie S, Wang J, Chang L, Yu Q, Zhan Z, Chen F (2017) Hydrogeochemistry and geothermometry of deep thermal water in the carbonate formation in the main urban area of Chongqing, China. J Hydrol 549:50–61. https://doi.org/10.1016/j.jhydrol.2017.03.054

Yao T, Thmpson LG, Mosley-Thompson E, Yang Z (1996) Climatological significance of $\delta^{18}O$ in north Tibetan ice cores. J Geophys Res Atmos 101:29531–29537. https://doi.org/10.1029/96JD02683

Zeng M (2012) Distribution and genesis of Chongqing hot spring. Master Thesis, Chengdu University of Technology (In Chinese with English abstract)

Zheng K, Han Z, Zhang Z (2010) Steady industrialized development of geothermal energy in China, In: Proceedings of the 2010 world geothermal congress, Bali, Indonesia, pp 25–29

Zhou X, Jin X, Liang S, Shen Y, Zhang H (2010) Monograph of groundwater sciences. Geological Publishing House, Beijing (in Chinese without English abstraction)